

# Tungusite: new data, relationship with gyrolite and structural model

GIOVANNI FERRARIS

Dip. Scienze Mineralogiche e Petrologiche, Univ. Torino, Via Valperga Caluso 37, 10125 Torino, Italy

ALESSANDRO PAVESE

Dip. Scienze della Terra, Sez. Mineralogia, Univ. Milano, Via Botticelli 23, 20133 Milano, Italy

AND

SVETLANA V. SOBOLEVA

Inst. Ore Deposits, Petrography, Mineralogy and Geochemistry, Russian Acad. Sci., Staromonetny per. 35, Moscow, Russia

## Abstract

New chemical analyses, electron and X-ray powder diffraction data, and comparison with gyrolite and reyerite show that tungusite has the ideal formula  $[\text{Ca}_{14}(\text{OH})_8](\text{Si}_8\text{O}_{20})(\text{Si}_8\text{O}_{20})_2[\text{Fe}^{2+}(\text{OH})_{14}]$ , symmetry  $P\bar{1}$  and  $a = 9.714(9)$ ,  $b = 9.721(9)$ ,  $c = 22.09(3)$ ,  $\alpha = 90.13(1)^\circ$ ,  $\beta = 98.3(2)^\circ$ ,  $\gamma = 120.0(1)^\circ$ ,  $Z = 1$ . A structural model for tungusite is derived by splitting the double tetrahedral layer of reyerite and inserting a trioctahedral X sheet which is ideally occupied by  $\text{Fe}^{2+}$ . Polytypism phenomena due to different relative positions between tetrahedral and X sheets are discussed. A substitutional solid solution represented by the formula  $[\text{Ca}_{14}(\text{OH})_8]\text{Si}_{24-y}\text{Al}_y\text{O}_{60}[\text{Na}_x\text{M}_{9-(x+z)}\square_z(\text{OH})_{14-(x+y+2z)}(x+y+2z)\text{H}_2\text{O}]$  includes tungusite ( $x = y = z = 0$ ,  $M = \text{Fe}^{2+}$ ) and gyrolite ( $x = 1$ ,  $y = 1$ ,  $z = 6$ ,  $M = \text{Ca}$ ).

KEYWORDS: tungusite, reyerite, gyrolite, structural model.

## Introduction

TUNGUSITE is a hydrous silicate of Ca and Fe described by Kudriashova (1966) using green chlorite-like flakes (up to 0.5 cm in diameter) from cavities of spherulitic lava collected on the right bank of the Lower Tunguska river (Tura, East Siberia). Anastasenko (1978) reported further findings within basalts of the North-West Siberian platform (basins of rivers Eramchino, Tutonchana and Kureyka). The mineral is associated with calcite, quartz, gyrolite, reyerite, datolite, apophyllite, analcime and unidentified zeolites. According to Kudriashova (1966), several supposed chlorites (particularly delessite) reported in similar associations may be tungusite.

The colour of tungusite varies from light-green to grass- and dark-green with increasing Fe-content; the radially fibrous flakes divide easily into lamellae

showing a very good {001} cleavage. The mineral was characterized (Anastasenko, 1978; Kudriashova, 1966) through: (1) optical data; (2) wet chemical analyses plus DTA and TGA (Table 1) leading to an ideal composition  $\text{Ca}_4\text{Si}_6\text{O}_{15}(\text{OH})_2 \cdot 2\text{Fe}(\text{OH})_2$ ; (3) using an unindexed powder pattern quite similar to that of gyrolite; (4) IR; and (5) Mössbauer spectra; the latter spectrum shows the presence of both ferric and ferrous iron.

New chemical analyses, X-ray powder pattern, electron diffraction data (selected area and oblique-texture patterns), and a structural model are reported in this paper. The hypothesis suggested by Kudriashova (1966), on the basis of powder pattern and chemical data, of a close structural relationship between tungusite and gyrolite, and the structure determination by Merlino (1988b) of the latter phase, provide the key to interpreting the experimental data of tungusite.

TABLE 1. Chemical analyses of tungusite. Oxides (top) and cation contents (bottom), for a formula unit, within the *O*, *S* and *X* sheets. Minimum and maximum values of the oxides are shown in each second line

	(1)	(2)	(3)
SiO <sub>2</sub>	46.31	49.65 (46.82–50.98)	47.41 (45.34–49.55)
Al <sub>2</sub> O <sub>3</sub>	2.93	1.67 (1.15–4.21)	1.88 (0.0–4.01)
FeO	11.52	7.59 (4.93–9.73)	12.44 (10.10–14.84)
Fe <sub>2</sub> O <sub>3</sub>	1.81	–	–
MgO	1.07	0.34 (0.0–0.56)	0.64 (0.0–1.12)
MnO	–	1.07 (0.59–1.66)	1.65 (0.0–2.25)
CaO	25.22	28.72 (25.14–30.23)	26.24 (24.11–27.97)
Na <sub>2</sub> O	1.91	0.29 (0.0–0.79)	0.47 (0.0–0.83)
K <sub>2</sub> O	–	0.13 (0.0–1.05)	0.28 (0.0–1.20)
H <sub>2</sub> O	7.92	–	–
Sum	98.69	89.46 (90.60–91.12)	91.01 (90.01–92.08)
<i>O</i> Ca	12.17	14.00	13.60
Mg	0.79		0.40
Na	1.04		
Sum	14.00	14.00	14.00
<i>S</i> Si	22.83	23.08	22.93
Al	1.70	0.92	1.07
Sum	24.53	24.00	24.00
<i>X</i> Ca	1.15	0.30	–
Na	0.79	0.26	0.44
K	–	0.08	0.17
Mg	0.79	0.24	0.06
Fe <sup>2+</sup>	4.75	2.95	5.03
Fe <sup>3+</sup>	0.67	–	–
Mn	–	0.42	0.68
Sum	7.36	4.25	6.38
OH	17.98	–	–
H <sub>2</sub> O	4.03	–	–

(1) (Kudriashova, 1966) – Average of two wet analyses; cations on the basis of 82 oxygens p.f.u. (see text).

(2), (3) (Present work) – Average microprobe analyses (anhydrous part) for samples with Fe content below [(2), 16 analyses] and above 4 atoms p.f.u. [(3), 40 analyses]. Cations on the basis of Si + Al = 24 p.f.u. (see text).

## Experimental

The samples used for this study have been kindly provided by V.I. Kudriashova from the original locality on the Lower Tunguska river. The apophyllite associated with tungusite (Kudriashova, 1966) has been identified as fluorapophyllite on the basis of the cell parameters obtained from single-crystal diffractometry:  $a = 8.94(2)$ ,  $c = 15.77(4)$  Å.

*Chemical analyses.* All examined samples of tungusite contain, at microscopic level, intergrowths of gyrolite and reyerite (Fig. 1). Besides, the content of Fe in the studied samples of tungusite is variable: from practically absent in the so called white tungusite, the Fe increases with darkening of the green colour.

In Table 1 the wet chemical analysis given by Kudriashova (1966) and our electron microprobe analyses are reported. The variable content of Fe in tungusite will be discussed below on a structural basis. In particular, the number of Fe atoms p.f.u. has never been found to be lower than about 2 and a statistical analysis of 56 chemical analyses shows a bimodal distribution with maxima near 3 and 5, the majority being nearer to 5. Consequently, in Table 1, average values of the data are presented for two different ranges of FeO. The microprobe analyses were obtained under the following conditions: SEM Cambridge S-360 equipped with EDS 860-Link System, 15 kV, 500 pA; standards were Ca(SiO<sub>3</sub>) (Ca), Fe<sub>2</sub>O<sub>3</sub> (Fe), MgO (Mg), MnCO<sub>3</sub> (Mn), NaCl (Na); KCl (K), Al<sub>2</sub>O<sub>3</sub> (Al), SiO<sub>2</sub> (Si); data reduction with ZAF4 (Duncumb and Reed, 1968).

*Electron diffraction.* Observation of tungusite under a transmission electron microscope (TEM; Philips CM12 equipped with EDAX PV9800) shows an irregular hexagonal contour of the single lamellae.

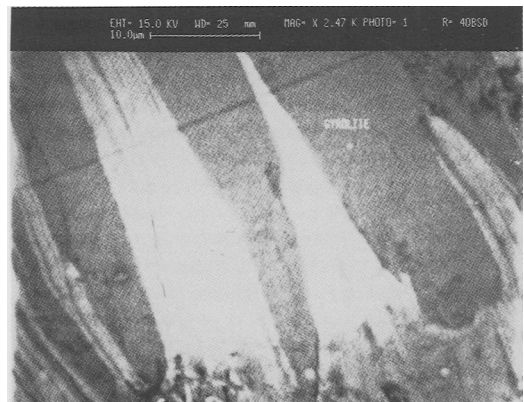


Fig. 1. Back scattered electron image of a sample where tungusite (light grey) is intergrown with gyrolite (dark grey).

Semi-quantitative data obtained with the EDAX facility confirmed the electron microprobe data and, in particular, showed the presence of Fe only as a component of tungusite and never as an impurity.

Basic crystallographic features of tungusite have been obtained through the electron diffraction oblique-texture method. In this method (Vainshtein, 1964; Zvyagin, 1967), by using an oblique incident beam of electrons, lamellae which lie parallel to the microscope stage and are randomly rotated around their common perpendicular produce diffraction spots which are characteristically distributed on different ellipses. For (001) lamellae, each ellipse contains reflections with constant  $h$  and  $k$  values and distances  $D$  from the small axis given by  $D = hp + ks + lq$ ; for a monoclinic cell,  $p = L\lambda/(a \cdot \tan\beta)$ ,  $s = 0$  and  $q = L\lambda/(c \cdot \sin\beta)$  ( $L$  is the distance between sample and film;  $\lambda$  is the wavelength of the radiation). Indexing of the oblique-texture pattern leads to an apparently monoclinic  $C$  cell with  $a' = \sqrt{3}b = 16.8 \text{ \AA}$ ,  $c = 22.0 \text{ \AA}$ ,  $\beta = \pm 100^\circ$ . This cell (with  $\beta = 100^\circ$ , see below) is used in this study except when otherwise stated; it has the same metrically hexagonal base which occurs in gyrolite and reyerite (Merlino, 1988*a,b*). Most of the oblique texture patterns of tungusite show practically continuous ellipses revealing a widespread disorder in the structure.

Selected area electron diffraction (SAED), with the beam perpendicular to the lamellae (along  $c^*$ ), shows bidimensional patterns which, in first approximation, are not only metrically but also symmetrically hexagonal; the bidimensional  $c$  lattice with  $a' = \sqrt{3}b = 16.8 \text{ \AA}$  found with oblique-texture patterns is confirmed (the presence of fluorapophyllite was used as an internal standard).

The observed SAED pattern is the intersection of the (001) cleavage plane with the reciprocal lattice. At the first approximation the intersection plane is perpendicular to [104] and should contain only ( $h = \pm 4n$ )  $k$  ( $l = \pm n$ ) reflections. However, because of the short length of  $c^*$ , disorder (stacking faults) along [001] and very small thickness of the lamellae, for  $-2 \leq l \leq 2$  the SAED pattern also contains reflections with  $h \neq \pm 4n$ .

*X-ray diffraction.* No single crystals suitable for X-ray diffraction have been found. Because of microscopic intergrowths of tungusite with gyrolite and reyerite, in the powder pattern the most intense reflections from the two latter phases are also present (Table 2); besides, the lamellar morphology favours preferential orientation, which is particularly evident when a flat sample is used. A powder diffraction pattern quite free of preferential orientation has been obtained with an INEL CPS 120 diffractometer, using material selected by a magnetic separator (Fe is absent in gyrolite and reyerite) within a glass capillary (Cu-K $\alpha$ ,  $\lambda = 1.5418 \text{ \AA}$ , graphite monochromator).

Tungusite was discovered to be triclinic and the following cell parameters were obtained from a least-squares refinement of the powder pattern (Table 2):  $a = 9.714(9)$ ,  $b = 9.721(9)$ ,  $c = 22.09(3) \text{ \AA}$ ,  $\alpha = 90.13(1)^\circ$ ,  $\beta = 98.3(2)^\circ$  and  $\gamma = 120.0(1)^\circ$ . Comparison with the powder pattern of tungusite reported by Kudriashova (1966) reveals discrepancies for large  $d_{hkl}$ , presumably because of zero point error in the older data.

## Discussion

*The structure of reyerite and gyrolite.* A strict relationship between the crystal structure of reyerite [ $\text{Ca}_{14}(\text{Na},\text{K})_2\text{Si}_{22}\text{Al}_2\text{O}_{58}(\text{OH})_8 \cdot 6\text{H}_2\text{O}$ ,  $a = 9.765$ ,  $c = 19.067 \text{ \AA}$ , space group  $P\bar{3}$ ,  $Z = 1$ ] and of gyrolite [ $\text{Ca}_{16}\text{NaSi}_{23}\text{AlO}_{60}(\text{OH})_8 \cdot 14\text{H}_2\text{O}$ ,  $a = b = 9.74$ ,  $c = 22.40 \text{ \AA}$ ,  $\alpha = 95.7$ ,  $\beta = 91.5$ ,  $\gamma = 120.0^\circ$ ; space group  $P\bar{1}$ ,  $Z = 1$ ] has been shown by Merlino (1988*a,b*).

The structure of gyrolite (cf. Fig. 2) differs from that of reyerite only by the presence of three (Ca,Na)-octahedra in a sheet ( $X$ ) between the tetrahedral sheets  $S_2$  and  $\bar{S}_2$  which, in the latter mineral, are directly connected to form a double layer. This addition accounts for the only substantial difference in composition between the two minerals:  $(\text{Ca},\text{Na})\text{O}_2 \cdot 8\text{H}_2\text{O}$ . Octahedral ( $O$ ) sheets of edge-sharing Ca-octahedra and a further type ( $S_1$ ) of tetrahedral sheet complete the structure of gyrolite. Both  $S_1$  and  $S_2$  sheets are built up by six-membered rings of tetrahedra pointing upwards and downwards in the ratio 1:1 and 3:1 for  $S_1$  and  $S_2$ , respectively. In first approximation  $O$  and  $S$  sheets maintain in gyrolite the trigonal symmetry of reyerite.

*Model of the structure.* An analysis of the available data shows that (1) the cell of tungusite is very close to that of gyrolite and along  $c^*$  differs from that of reyerite by about  $2.8 \text{ \AA}$ ; (2) the chemical composition of the anhydrous part of tungusite differs from that of gyrolite by the presence of Fe only; (3) the difference along  $c^*$  ( $2.8 \text{ \AA}$ ) and the dimensions of the triclinic cell base ( $a \approx b = 9.72 \text{ \AA}$ ,  $\gamma = 120^\circ$ ) correspond to those of a  $3 \times 3$  brucite-like trioctahedral sheet. By assuming that the same framework of oxygens [ $60 \text{ O} + 8 \text{ OH} + 14(\text{OH},\text{H}_2\text{O})$ ] is present both in gyrolite and tungusite and the  $X$  sheet, which in gyrolite contains only 3(Ca, Na), can be filled up to nine cations, the following ideal content of the unit cell is obtained for tungusite:  $[\text{Ca}_{14}(\text{OH})_8](\text{Si}_8\text{O}_{20})(\text{Si}_8\text{O}_{20})_2 - [\text{M}_9^+(\text{OH})_{14}]$ . This formula compares favourably with the atomic composition obtained from the chemical analyses in Table 1.

On this basis, and taking into account the possible polytypes, the model of tungusite shown in Fig. 2 is obtained. It corresponds to the polytype with a shift  $-\frac{2}{3}a'$  of the complex layer  $\bar{S}_2\bar{O}S_1$  (see below) and with the approximate atomic coordinates given in

TABLE 2. X-ray powder pattern of tungusite;  $d_{\text{obs.}}$  and  $d_{\text{calc.}}$  refer to experimental and calculated interplanar distances;  $I_{\text{obs.}}$  and  $I_{\text{calc.}}$  refer to the corresponding observed and calculated intensities on a relative scale (maximum value = 100). The reflections not used for the refinement of the triclinic cell are starred

$I_{\text{obs.}}$	$I_{\text{calc.}}$	$d_{\text{obs.}}$	$d_{\text{calc.}}$	$h k l$
20		22.20	22.20	0 0 1 (gyrolite)
7		18.88	19.07	0 0 1 (reyerite)
3		11.17	11.10	0 0 2 (gyrolite)
7		9.62	9.66	0 0 2 (reyerite)
9	1	8.45	8.39; 8.39	-1 1 0; 0 1 0
33	22	7.22	7.26	0 0 3
3	1	6.31	6.38; 6.39	0 1 2*; 1 -1 2*
23	20	5.40	5.44	0 0 4
7	1	4.77	4.80; 4.81; 4.74	-1 -1 0; -2 1 0; 1 -2 -1
30	20	4.31	4.35	0 0 5
62	32	4.20	4.20; 4.19; 4.19	-2 0 1; -2 2 0; 0 -2 0
			4.19; 4.18	0 -2 1; 2 -2 -1
13	3	3.813	3.808; 3.802	2 -2 2; 0 2 2*
100	63	3.591	3.629	0 0 6
72	47	3.145	3.154; 3.152	1 2 0; -3 1 2
			3.132	2 -3 1*
25	30	3.037	3.065; 3.064	1 2 1; -3 1 3
27	13	2.856	2.881	2 -3 3
25	25	2.800	2.796; 2.795; 2.794	-3 3 0; 0 3 0; -3 0 2
25	100	2.746	2.765; 2.763; 2.741	1 2 3; -3 1 5; -3 0 3
			2.743; 2.744; 2.711	0 3 1; 3 -3 1; 2 -3 4*
34	36	2.655	2.652; 2.655; 2.651	0 3 2; 3 -3 2; -3 0 4
8	53	2.538	2.539; 2.535; 2.535	3 -3 3; 0 -3 -3; 3 0 -5
10	47	2.398	2.419; 2.403; 2.407	0 0 9; 0 3 4; 3 -3 4
			2.403	-3 0 6
7	2	2.334	2.334; 2.331	-4 3 1; 1 -4 1
17	35	2.252	2.264; 2.264; 2.240	0 3 5; -3 0 7; 1 2 6
			2.240	-3 1 8
10	10	2.194	2.191	2 -3 7
11	40	2.098	2.127; 2.126; 2.129	-3 0 8*; 0 3 6*; 3 -3 6*
11	27	2.074	2.083; 2.083	1 2 7; -3 1 9
8	23	1.981	1.994; 1.998; 1.995	0 3 7; 3 -3 7; -3 0 9
8	10	1.927	1.914; 1.912	0 -3 9; 3 0 7
74	70	1.837	1.836; 1.836; 1.837	-4 -1 2; -5 4 1; 1 -5 1
			1.833; 1.833	1 -5 0; 5 -4 -2
13	18	1.810	1.810; 1.810; 1.810	-5 1 0; 4 1 0; -4 -1 4
			1.810; 1.809	1 2 9; 3 -1 -11
11	21	1.766	1.758; 1.755; 1.755	3 -3 9; 0 3 9; -3 0 11
17	39	1.616	1.615; 1.614; 1.615	-6 3 1; -3 -3 1; -3 6 1
			1.614; 1.615	-6 3 3; -3 -3 3
14	30	1.602	1.602; 1.602; 1.603	-6 3 0; -3 6 2; 3 -6 2
			1.601; 1.602; 1.602	-6 3 4; -3 -3 4; -3 -3 0
26	21	1.580	1.581; 1.581; 1.581	6 -3 1; -3 -3 5; -3 6 3

Table 3. This model is based on the triclinic cell reported above (space group  $P\bar{1}$ ); the single sheets (including the X sheet) approximately show trigonal symmetry as in gyrolite. The reliability of the structural model proposed for tungusite is supported

by its capacity to explain (1) crystallographic and chemical data, (2) the existence of a gyrolite-tungusite substitutional solid solution (see below) and by (3) the reasonable agreement between calculated and experimental diffraction intensities

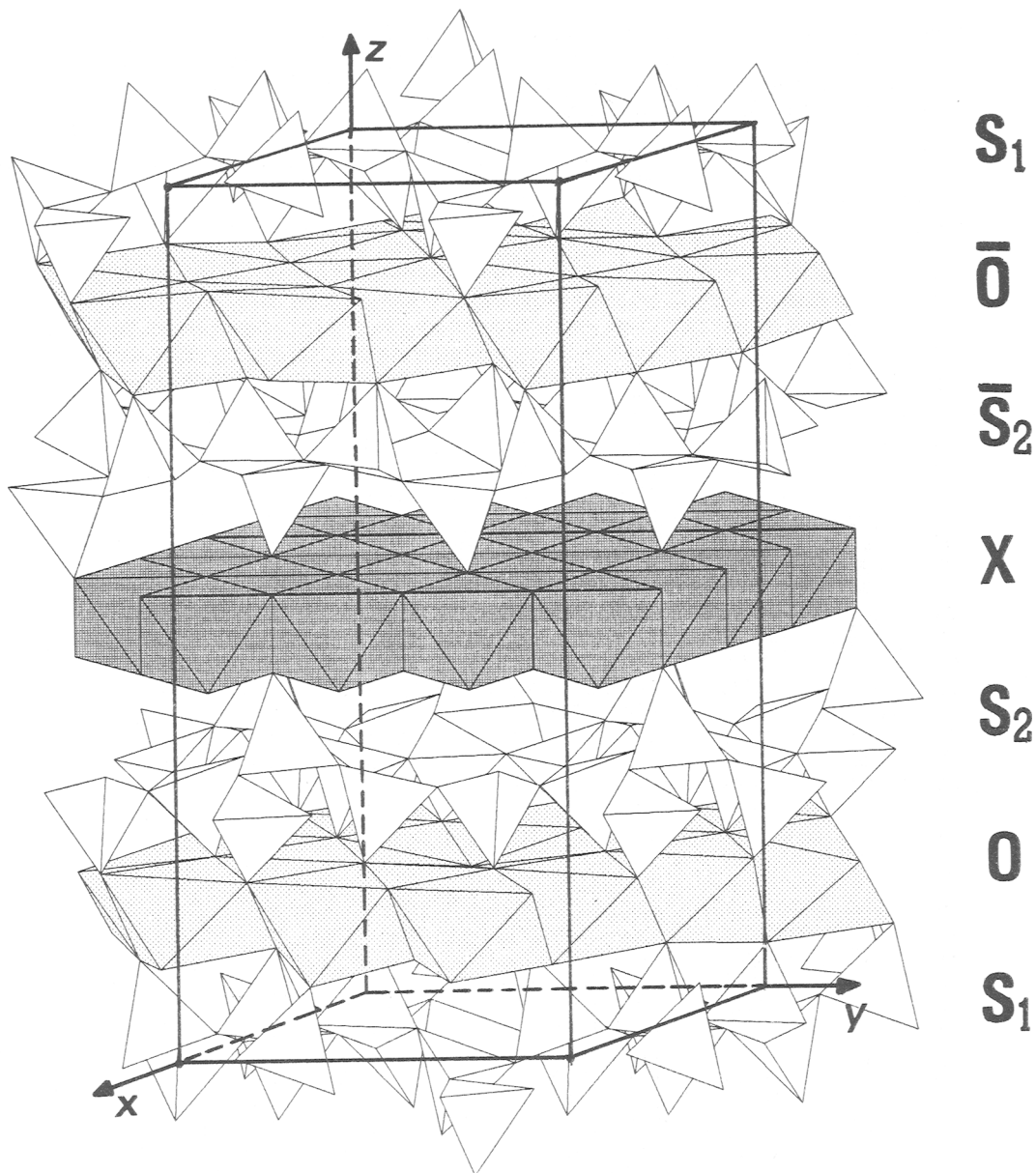


Fig. 2. Perspective view along [100] of the crystal structure of tungusite.

for the X-ray powder pattern (Table 2). To evaluate this agreement it should be kept in mind that the structural model is based on a fully occupied X sheet and has not been refined: small variations of positional and thermal parameters can have great influence on single intensities, particularly for high- $\theta$  reflections. In fact, even with some kind of constraint, in order to decrease the large number of structural parameters, a reliable Rietveld refinement

of the powder pattern proved to be an impossible task if only for the following reasons: (1) the experimental data contain some contributions from gyrolite and reyerite which are intergrown with tungusite at microscopic level (Fig.1, Table 2); and (2) as shown by oblique-texture electron-diffraction patterns, tungusite is strongly disordered because of stacking faults which presumably arise from the coexistence of different polytypes (see below).

TABLE 3. Atomic fractional coordinates of tungusite in triclinic setting. Atoms labelled with 0 as the last digit correspond to independent positions in reyerite (Merlino, 1988a); other atoms correspond to those generated by the threefold axis in reyerite or to the Fe filling the octahedral X sheet

Ca10	0.742	0.371	0.169	O70	0.253	0.234	-0.020
Ca20	0.310	0.083	0.149	O71	-0.247	0.020	-0.020
Ca21	0.016	0.227	0.149	O72	-0.033	-0.267	-0.020
Ca22	-0.127	-0.211	0.149	O80	0.327	0.509	0.022
Ca30	0.463	0.515	0.173	O81	-0.495	-0.185	0.022
Ca31	-0.399	-0.052	0.173	O82	0.200	-0.313	0.022
Ca32	0.167	-0.348	0.173	O90	0.380	0.371	0.301
Si10	0.224	0.322	0.034	O91	-0.170	0.009	0.301
Si11	-0.299	-0.098	0.034	O92	0.192	-0.179	0.301
Si12	0.121	-0.201	0.034	O101	0.402	0.117	0.303
Si20	0.355	0.678	0.050	O102	0.085	0.285	0.303
Si30	0.492	0.301	0.288	O103	-0.083	-0.200	0.303
Si31	-0.110	0.190	0.288	O110	0.529	0.765	0.441
Si32	0.001	-0.300	0.288	O120	0.311	0.582	0.335
Si40	0.252	0.431	0.288	O121	-0.359	-0.271	0.335
Si41	-0.239	-0.179	0.288	O122	0.494	-0.088	0.335
Si42	0.371	-0.059	0.288	O130	0.658	0.402	0.336
Si50	0.828	0.414	0.362	O131	-0.178	0.256	0.336
Al10	0.495	0.747	0.363	O132	-0.032	-0.434	0.336
O10	0.262	0.285	0.103	O111	0.196	0.098	0.441
O11	-0.216	-0.024	0.103	O112	0.196	0.431	0.441
O12	0.092	-0.193	0.103	O113	0.196	-0.235	0.441
O20	0.543	0.123	0.118	O114	0.529	0.431	0.441
O21	-0.045	0.420	0.118	O115	0.529	0.098	0.441
O22	-0.341	-0.465	0.118	O116	-0.137	0.431	0.441
O30	0.230	0.462	0.217	O117	-0.137	-0.235	0.441
O31	-0.317	-0.232	0.217	O118	-0.137	0.098	0.441
O32	0.376	-0.086	0.217	Fe1	0.000	0.000	0.500
O40	0.516	0.316	0.217	Fe2	0.000	0.333	0.500
O41	-0.171	0.200	0.217	Fe3	0.333	0.000	0.500
O42	-0.055	-0.371	0.217	Fe4	0.333	0.333	0.500
O50	0.086	0.043	0.192	Fe5	0.333	-0.333	0.500
O60	0.388	0.694	0.123				

*Thermal behaviour.* Comparison of the TGA data published by Kudriashova (1966) for tungusite with those published for gyrolite by Garavelli and Vurro (1984) allows some conclusions on the basis of the crystal structures. The main differences between the two TGA patterns are (1) a loss of  $\sim 6\%$  in weight below  $100^\circ\text{C}$  in gyrolite against a negligible amount in tungusite; (2) a shift of the last step of weight loss from  $550^\circ\text{C}$  in gyrolite to  $650^\circ\text{C}$  in tungusite. The former is connected with the lack (or a minor presence) of weakly bonded water in the X sheet of tungusite. The last step in TGA is connected with the collapse of the structure; this reasonably should begin in the X sheet which links the two  $S_1O_5S_2$  layers more strongly in tungusite (octahedral X sheet) than in gyrolite (isolated Ca/Na octahedra).

The DTA of tungusite (Kudriashova, 1966) shows two exothermic reactions which can be interpreted as oxidation of  $\text{Fe}^{2+}$  to  $\text{Fe}^{3+}$  ( $320^\circ\text{C}$ ) and formation of wollastonite ( $\alpha\text{-CaSiO}_3$ ) after the collapse of the structure ( $850^\circ\text{C}$ ); the latter event is also present in gyrolite (Garavelli and Vurro, 1984).

*Crystal chemistry and the gyrolite-tungusite series.* According to the structural model of tungusite, the cation contents of the chemical analyses (Table 1) are calculated on the basis of 82 oxygens p.f.u. when the water content is known, and of  $\text{Si} + \text{Al} = 24$  in the case of microprobe analyses (anhydrous part only).

In agreement with evidence from the refinement of the structure, in gyrolite (Merlino, 1988b) the O sheet was filled with 14 Ca, whereas Na (about 1 atom)

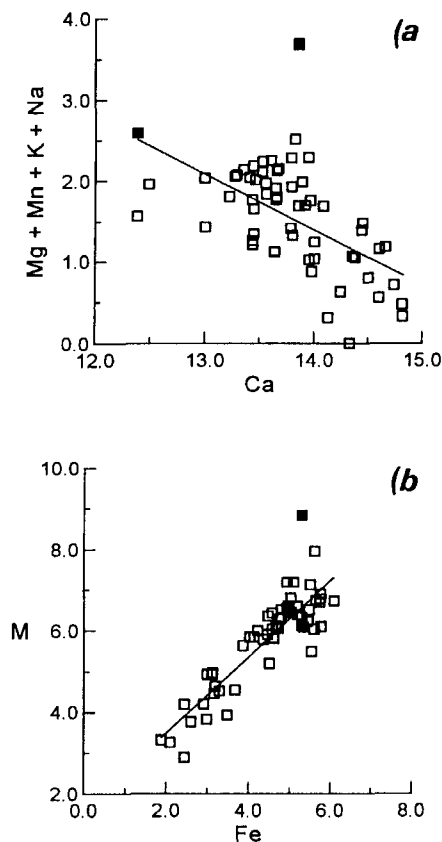


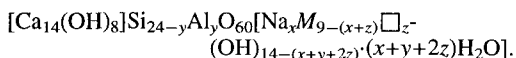
FIG. 3. Plot of the atomic contents p.f.u. of (a) Na+K+Mg+Mn vs. Ca; and (b) of the number  $M$  of cations in the  $X$  sheet vs. Fe. Full squares represent Kudriashova's (1966) analyses.

was put in the  $X$  sheet. Even if the small amount of K found in the analyses (Table 1) is included in the following discussion, it is possibly due to reyerite impurities, because this cation can not be easily accommodated in the  $X$  layer. The plots of Fig. 3 and also the average values (Table 1) show that in some individual chemical analyses of tungusite the quantity of Ca is not enough to fill the  $O$  sheet. Correlation between the relative numbers of cations reveals that  $(\text{Na} + \text{K} + \text{Mg} + \text{Mn})$  decreases with Ca (Fig. 3a); besides, the total number of octahedral cations minus Fe ( $\Sigma_{\text{oct}} - \text{Fe}$ ) is quite constant and close to 15.5 atoms p.f.u. (Table 1). This means that there is a one-to-one substitution between the non-Fe octahedral cations and Ca. To obtain the 14 cations which are necessary to fill the  $O$  sheet when  $\text{Ca} < 14$ , Mg and Na are used in order of preference. In fact, Mg usually shows a fairly regular octahedral

coordination and, therefore, is more suitable to complete the quite regular octahedral  $O$  sheet. Consequently, the number  $M$  of cations in the  $X$  sheet is obtained from  $\Sigma_{\text{oct}}$  by subtracting the  $14(\text{Ca} + \text{Mg} + \text{Na})$  cations which are necessary to fill the  $O$  sheet. In the  $X$  sheet,  $M$  ranges approximately from 2 to 9 and increases with the content of Fe (Fig. 3b). The sample with the largest value of  $M$  (8.8 with 5.3 Fe) has been reported by Kudriashova (1966); from the present work, the lowest and highest values of  $M$  are 3.4 (1.8 Fe) and 6.7 (6.1 Fe) atoms p.f.u., respectively. Since Ca tends to be absent in the  $X$  sheet, where some Na can still occur, the minimum content of about 2 Fe atoms p.f.u. can be interpreted in the following way: (1) in an environment rich in Fe, this element is more suitable than Ca to enter the  $X$  sheet; (2) the minimum content of this sheet must be 3 cations (including Na) in order to ensure a gyrolite-like structure, otherwise the sheet would collapse down to a reyerite-like structure.

Because of the variability in the number and the charge of the cations in the  $X$  sheet, the  $14(\text{OH})^-$  which are ideally present in the structure of tungusite can be (in part) replaced by  $\text{H}_2\text{O}$  to provide charge balance. The main substitutions acting in the gyrolite-like structure are:  $\text{Ca} = \text{Fe}^{2+}$  (to a limited extent) and  $\square + 2\text{H}_2\text{O} = \text{Fe}^{2+} + 2\text{OH}^-$  (with the loss of  $2\text{H}^+$ ); a minor substitution can also be  $3\text{Fe}^{2+} = 2\text{Fe}^{3+} + \square$ .

On the basis of the previous discussion, the following formula is proposed to account for the chemical variability of tungusite and the existence of a substitutional solid solution which includes gyrolite (Merlino 1988b;  $M = \text{Ca}$ ,  $x = 1$ ,  $y = 1$ ,  $z = 6$ ) and tungusite ( $M = \text{Fe}^{2+}$ ,  $x = 1$ ,  $y = 1$ ,  $z = 0$  according to analyses of Table 1 or, ideally,  $x = y = z = 0$ ):



Taking into account the contents of the  $X$  sheet, in the gyrolite-tungusite series the name gyrolite is applied to members with Ca dominant in the  $X$  sheet and the name tungusite is reserved to members with Fe dominant in the same sheet. The reported 'white-tungusite' (Anastassenko, 1978) is Fe-bearing gyrolite as, possibly, is some of the 'light-green tungusite'; however, likely most of the latter is Fe-poor tungusite.

*Polytypism, stacking disorder.* The tetrahedral  $S_1$  and  $S_2$  sheets which sandwich the octahedral  $O$  sheet (Fig. 2) are structurally different and, therefore, as already noted by Merlino (1988a), polytypes due to different mutual attachments of the  $S_1$  and  $S_2$  sheets to the  $O$  sheet are not likely. Instead, structurally equivalent complex  $S_1\text{O}S_2$  layers are attached on both sides of the  $X$  sheet. On each side of the  $X$  sheet two octahedral corners per primitive cell are shared

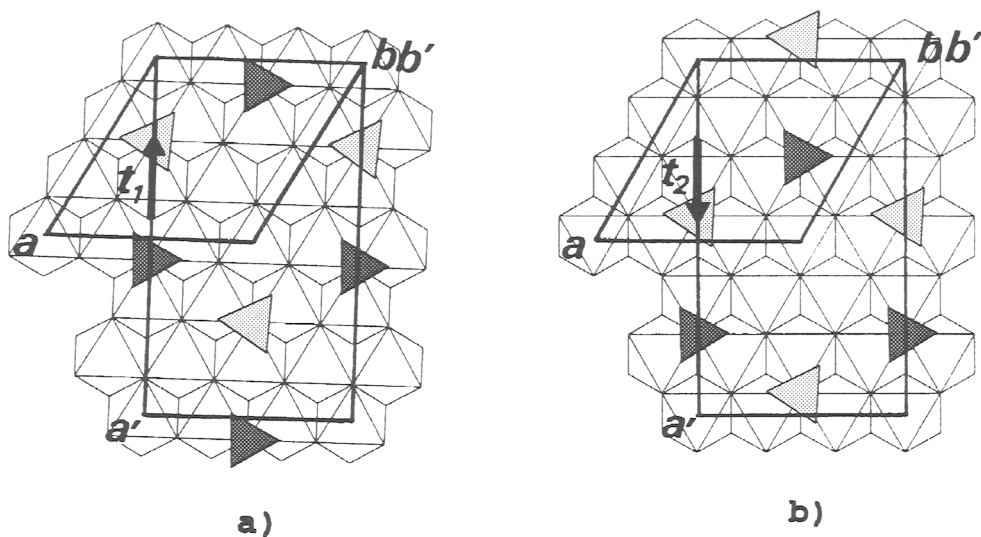


FIG. 4. Stagger vectors  $\mathbf{t}_1$  and  $\mathbf{t}_2$  for the two polytypes of tungusite discussed in the text. Only the tetrahedra attached on the top of the octahedral X sheet are shown. In polytype b the X sheet is rotated  $60^\circ$  with respect to polytype a.

with tetrahedra (Fig. 4). Shifts of one  $S_1OS_2$  layer with respect to that attached on the opposite side of the same X sheet can therefore be expected, as in other layer silicates. Such polytypes differ in the c stacking vector and are completely defined by stagger vectors  $\mathbf{t}$ , which represent the shifts of the layer  $S_1OS_2$  with respect to  $S_2OS_1$ .

The results from oblique-texture electron-diffraction and X-ray powder patterns show that in our samples two metrically indistinguishable polytypes are predominant, with cell parameters  $a' = 16.83$ ,  $c = 22.09$  Å and  $\beta = \pm 99.75^\circ$ . An inspection of the crystal structure reveals that the stagger vectors which are compatible with these two cells are  $\mathbf{t}_1 = -\frac{2}{3}\mathbf{a}'$ , and  $\mathbf{t}_2 = +\frac{2}{3}\mathbf{a}'$  (Fig. 4). In these two cases the orientation of the X sheet differs by  $60^\circ$ .

Calculation of the diffraction intensities for the two polytype models corresponding to the stagger vectors  $\mathbf{t}_1$  and  $\mathbf{t}_2$ , proved the structure generated by the first polytype (i.e. with shift  $-\frac{2}{3}\mathbf{a}'$ , Fig. 4a) to be more consistent with the experimental X-ray powder pattern (Table 2).

*Conditions of formation.* Tungusite occurs in the core of cavities within spherulitic lavas. Taking into account the data on the regional metamorphic process concerning the Lower Tunguska river (Reverdatto *et al.*, 1979) and on the experimental synthesis of gyrolite and reyerite (Meyer and Jaunarajs, 1961), it can be concluded that tungusite formed during the late stages of the post-effusive low-temperature

hydrothermal processes under the influence of trap magmas. Presumably, hot (about  $200^\circ\text{C}$ ) hydrothermal solutions rich in Si and Fe interacted with Ca rich diabases; with decreasing concentration of Fe, gyrolite and reyerite formed instead.

#### Acknowledgements

The research was supported by M.U.R.S.T. (Roma). The visit of S.V. Soboleva to Italy was funded by grants from M.A.E. (Roma) and Università degli Studi di Torino. The authors are grateful to V.I. Kudriashova for providing the samples of tungusite and to G. Artioli, G. Lucchetti and K. Ståhl for assistance with magnetic separation and powder data collection.

#### References

- Anastassenko, G. F. (1978) *Boron-bearing traps of the North-West Siberian platform*. Leningrad Univ. Press, Leningrad (in Russian).
- Duncumb, P. and Reed, S.J.B. (1968) The calculation of stopping power and back-scattered effects in electron probe analysis. In: *Quantitative electron probe microanalysis* (K.F.J. Heinrich, ed.) NBS spec. pub. 298.
- Garavelli, C.L. and Vurro, F. (1984) *Rend. Soc. Ital. Mineral. Petr.*, **39**, 695–704.
- Kudriashova, V.I. (1966) *Dokl. Akad. Nauk SSSR*, **171**,



- 1167–70. [*Mineral. Abstr.* XVIII, 206] (in Russian).
- Merlino, S. (1988a) *Mineral. Mag.*, **52**, 247–55.
- Merlino, S. (1988b) *Mineral. Mag.*, **52**, 377–87.
- Meyer, J.W. and Jaunarajs, J.L. (1961) *Amer. Mineral.*, **46**, 913–33.
- Reverdato, V.V., Pertzov, N.N. and Korolyuk, V.N. (1979) *Contrib. Mineral. Petrol.*, **70**, 203–8.
- Vainshtein, B.K. (1964) *Structure Analysis by Electron Diffraction*. Pergamon Press, Oxford.
- Zvyagin, B.B. (1967) *Electron Diffraction Analysis of Clay Mineral Structures*. Plenum Press, New York.

[Manuscript received 12 July 1994:  
revised 20 October 1994]